Available online at www.sciencedirect.com
ScienceDirect
Computer-Aided Design 41 (2009) 566–572
COMPUTER-AIDED DESIGN
www.elsevier.com/locate/cad

Hexahedral mesh development of free-formed geometry: The human femur exemplified

Alexandra Schonning[a,*], Binu Oommen[b], Irina Ionescu[c], Ted Conway[d]

[a] *Program of Mechanical Engineering, Room 50/2500, University of North Florida, 4567 St. Johns Bluff Road South, Jacksonville, FL 32224, USA*
[b] *Department of Materials Science and Engineering, Massachusetts Institute of Technology, Cambridge, MA 02139, USA*
[c] *Dartmouth College, Department of Radiology, Hanover, NH 03755, USA*
[d] *School of Education, Virginia Commonwealth University, Richmond, VA 23284, USA*

Received 6 April 2006; accepted 1 October 2007

Abstract

The objective of the present research is to develop a standard hexahedral Finite Element (FE) model of the human femur accounting for the material characteristics of cortical bone, cancellous bone and bone marrow. The anatomical data were acquired from the Visible Human Project. A detailed outline of the steps necessary in developing hexahedral FE meshes from computed tomography (CT) data is provided, along with a section on modelling strategies providing comprehensive suggestions on how to overcome meshing difficulties due to geometrical non-linearities. The stress and deformation results are discussed.
Published by Elsevier Ltd

Keywords: Hexahedral mesh; Finite element modelling; Human femur

1. Introduction

Advances in computer technology, scanning techniques, software packages and FE techniques are allowing for increasingly sophisticated, reliable and realistic FE models of human bones. FE modelling in biomechanics originated with modelling human bones based on X-ray and photographic information. The first FE model used to determine the stresses in human bone was developed in 1972 [1]. As CT emerged, hard tissue models were developed and in 1986 an isotropic model of the tibia was published [2]. Other scanning techniques have also been employed in obtaining data necessary for creating FE models of human bone. For example, MRI and ultrasound data are used to better understand stress distribution of a normal gait [3]. The FE models developed have numerous uses; they can predict the stress level in the bones, estimate the stress level in joints, and optimize implants.

Due to the complexity of anatomical geometry, tetrahedral elements are most commonly used in biomechanical applications [4–12] as the meshing process is automated. Hexahedral elements are preferred by many researchers to the tetrahedral elements. They require extensive manual meshing but provide significant benefits such as regularity, angle distribution and anisotropy [13]. In comparing linear tetrahedral and hexahedral elements it has been judged that hexahedral elements give better quality results in many structural applications [14,15], including linear static bending, linear static torsion, and non-linear elasto-plastic analysis [16]. The quadratic tetrahedral element has been found to be adequate for many structural applications; nevertheless hexahedral elements showed improved convergence and sensitivity to mesh orientation [14]. General contact problems perform better with linear as opposed to second order elements [17]. However, the effort attributed to developing a hexahedral mesh should be weighted against its advantages. Researchers have developed reasonably good hexahedral meshes of independent bones. For example, the tibia was modelled using CT data of subject-specific anatomies in [18]. The femoral head to the lesser trochanter of the femur was modelled of subject-specific femurs in a study comparing quantitative CT to dual energy X-ray absorptiometry [19]. The proximal femur was modelled to study the load transfer characteristics of cemented hip replacements [20]. In yet another study, subject-specific femoral models were generated to test the robustness of an automatic mesh generator [21]. Also, the influence of muscle

* Corresponding author. Tel.: +1 904 620 2357; fax: +1 904 620 1391.
E-mail address: aschonni@unf.edu (A. Schonning).

0010-4485/$ - see front matter. Published by Elsevier Ltd
doi:10.1016/j.cad.2007.10.007

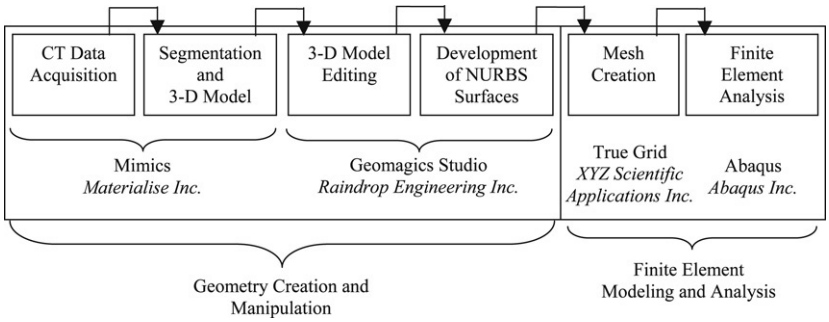

Fig. 1. Model development process outline.

forces on the femoral strain distribution was studied with a hexahedral model [22], and portions of the femur were modelled in an effort to study a Gamma nail within a fractured femur [23].

While progress has been made in the development of hexahedral FE models of the femur, many of the existing hexahedral models are based on patient-specific anatomies unavailable to other researchers; they may not include the complete femur or are used for specific studies not providing the stress results for a standard loading scenario. By contrast, in the present study, an adaptable hexahedral mesh was developed to utilize the advantages of the hexahedral elements. The anatomy was based on data readily available to others through the Visible Human Project [24], and includes the complete femur anatomy. Lastly, the results of this study may be useful to others conducting comparative analyses.

Furthermore, the FE models presented in literature generally target a specific application and don't provide much detail on how to reproduce similar meshes. Hexahedral meshes require an extensive amount of manual development resulting in much effort spent on learning how to develop them. In an effort to minimize the time spent on mesh generation, this paper provides detailed documentation of how the FE mesh was constructed. The procedure is exemplified for the case of a human femur, but can be adapted to any hard tissue structure making it a valuable resource to the biomechanics community.

2. Materials and methods

Several steps are involved in developing and analysing the hexahedral FE model of the femur. These include data acquisition, generation and editing of a three-dimensional model, generation of Non Uniform Rational B-Spline (NURBS) surfaces, mesh development and lastly FE analysis. Fig. 1 illustrates the methodology used for the model development process. Each of the steps is discussed in detail in the following subsections.

2.1. Data acquisition and three-dimensional model generation

The data was obtained from the National Institutes of Health's (NIH) Visible Human Project [24]. This CT data consisted of transversal images of the right femur of a human male, taken 1 mm apart. The density of the tissue can be calculated based on image intensity levels [25,26].

To perform the task of image segmentation, the CT data was imported into a medical imaging and editing software, in the present case Mimics (Materialize). Separate volumes were generated for the cortical bone, cancellous bone and the bone marrow. A semi-automated segmentation algorithm was used in conjunction with a region-growing algorithm applied to interpolate the 2D-image data, resulting in the generation of three-dimensional models.

2.2. Data smoothing and NURBS development

The volumes generated were edited further using a reverse- engineering software package called Geomagics Studio (Raindrop Engineering). The imported geometry had rough surfaces and included some inaccuracies (interpolation algorithms were used in estimating the surface between the 1 mm separated scans, threshold values were estimated in defining the boundary of the bony tissue, and editing techniques were used on slices). While some details were removed from the models through the available smoothing techniques, it aided in generating the FE mesh. Fig. 2 shows an image of the femoral head before and after smoothing operations.

To best prepare the geometry for meshing, the polygonal surface was replaced by a highly compliant NonUniform Rational B-Spline (NURBS) surface. It was comprised of rectangular patches, as shown in Fig. 3, which aided in the meshing process. For the model at hand, it was desired to create surface patches that could easily be "mapped" into block structures in the mesh generation software. The NURBS surface was exported as an *.iges file. The methodology described was carried out for the cortical, cancellous, and the bone marrow volumes.

2.3. Hexahedral mesh development

A commercial FE meshing software package (TrueGrid), using a multi-block approach that allows for the generation of highly controllable hexahedral meshes, was employed. This software was preferred as it is used as a preprocessor for a vast number of FE packages. The outline specified here may be of aid for mesh construction using other multi-block meshers. When using a multi-block mesher, the analyst divides the structure into manageable blocks. These blocks are then subdivided into elements. The subdivision of the geometry into manageable blocks will here be referred to as the block structure.

The development of a hexahedral mesh of the femur is complex for the following reasons: the femur cannot be

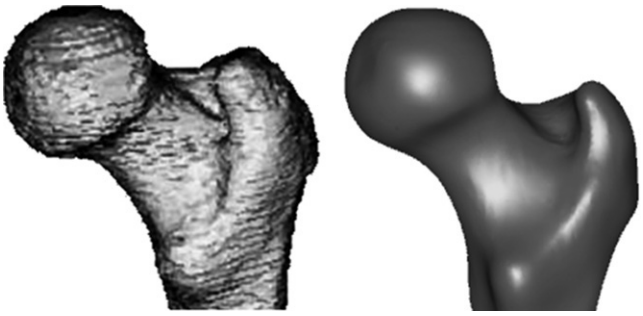

Fig. 2. Femoral head before and after smoothing.

simplified as a two-dimensional mesh extruded in the third direction; the femur consists of highly irregular external geometry (i.e. femoral head, greater trochanter, condyles) and complex inner structure.

The femur was modelled in four distinct steps; the first tackled the bone marrow, the second included the cancellous bone as well as part of the cortical bone along the diaphysis, the third step consisted of modelling the cortical bone around the femoral head, greater trochanter, condyles and the remaining cortical bone along the diaphysis; and the fourth and final step included merging eight extra blocks to the femoral structure. Each of these steps is described in the following subsections.

Step 1: Meshing of the medullar volume

The *.iges geometry of the bone marrow volume was imported into TrueGrid. A block structure was generated, as seen in Fig. 4(a). Each of the corners of the blocks was attached to the appropriate geometry vertices, followed by projection of the blocks' faces onto the geometry's "combined surfaces". Upon completion of the projection, the mesh density was increased to ensure that the projection was performed properly. The block mesh projected onto the marrow geometry is shown in Fig. 4(b).

Step 2: Meshing of the cancellous bone and the cortical bone along the diaphysis

In meshing the bone marrow, an input file of the commands was generated. The next step was to mesh the cancellous volume and the cortical volume along the diaphysis of the femur. In doing so, the bone marrow mesh file generated in Step 1 was modified to account for this additional volume. The primary modification to the file was to expand the block-structure, as shown in Fig. 4(c). This block structure also incorporates some of the cortical bone along the diaphysis of the femur as this simplified the block structure.

Fig. 4(d) shows the block structure attached to the geometry. This figure illustrates the mesh after all of the block-boundary commands had been applied, after the corners of the computational blocks had been attached to the vertices of the physical geometry, and after the faces of the blocks had been projected onto the "combined surfaces" of the geometrical structure. Where highly irregular geometry occurs it was necessary to also attach the edges of the block structure to the curves of the geometry. One location of highly irregular geometry occurs at the condyles. In studying the block structure of Fig. 4(c)–(d), it should be noted that the centre elements include the medullar volume. However, above and below the medullar volume are now blocks/elements that will be assigned material properties of cancellous bone. Blocks along the diaphysis will be assigned material properties of cortical bone.

Fig. 3. NURBS patch layout.

Step 3: Meshing the outer cortical shell

In developing the mesh for the cortical volume, modifications were made to the file developed in step 2. Blocks were added and in some cases blocks were subdivided to increase the controllability of the mesh. The complete block structure (with the exception of eight blocks described in step 4) is shown in Fig. 4(e).

As is shown, the block structure is now more complex. A layer of blocks was added in the superior and inferior directions to resemble the cortical volume, a layer of blocks was also added in the posterior/anterior and medial/lateral directions around the femoral diaphysis, and blocks were added on the posterior and anterior sides of the femoral head, greater trochanter and condyles. These extra blocks were then attached to each other using block-boundary commands, resulting in the mesh shown in Fig. 4(f). After increasing the mesh density the final mesh, seen in Fig. 4(g), was obtained.

To better describe how the block-boundary commands were used, a coloured image of the block region is shown in Fig. 5(a). The block-boundary command was applied to faces with the same colour. Some of the vertices are marked with coloured circles and those with the same colour make up the same node following completion of the block boundary and merging commands. For example, the two yellow faces are attached to each other; the two gray faces are attached to each other; and the two pink faces are attached to each other. As these faces attach, a common node develops and is marked by a grey circle. While not clearly shown in Fig. 5(a), the red face attaches to a face opposite to the pink face causing the four red nodes to merge into one. Fig. 5(b) shows the resulting (low density) mesh following completion of the block-boundary commands. In this figure, nodes are coloured to match the vertices in Fig. 5(a). A similar process was applied to the regions of the greater trochanter and condyles.

Step 4: Creation of the final eight blocks

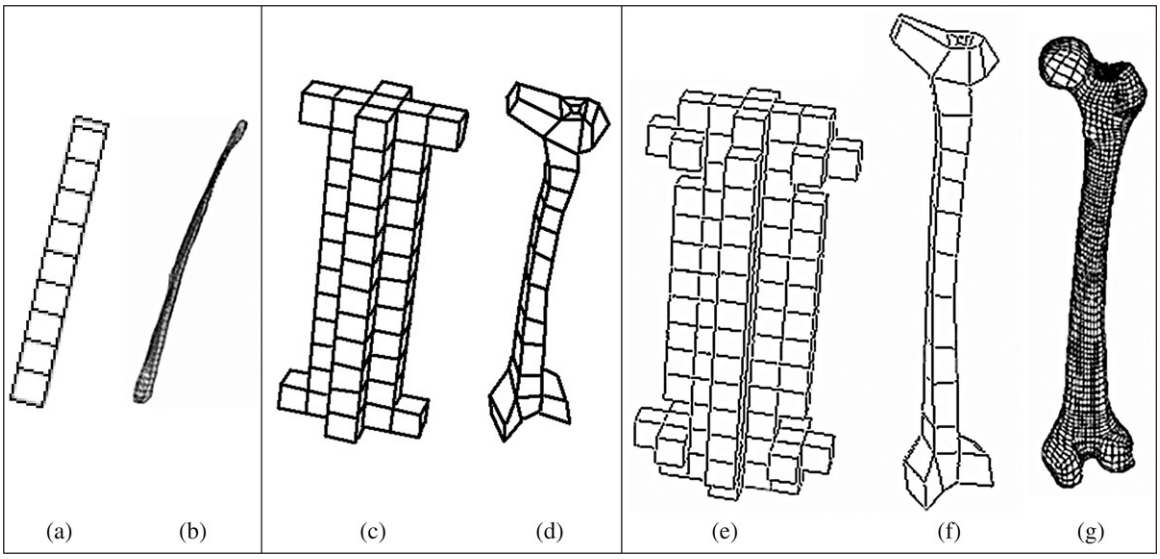

Fig. 4. Block-structure developed in Steps 1–3. Figure (a) shows the block structure of the bone marrow, and (b) shows the marrow block-structure projected onto the geometry. Figure (c) and (d) illustrate the block-structure of the cancellous volume and part of the cortical volume along the femoral diaphysis before and after bounding specific surfaces. In (e) is the cortical block structure after removing unnecessary blocks, (f) shows the same block structure after bounding specific faces, and (g) shows the resulting mesh following projection of the faces and subdivision into hexahedral elements.

As indicated in Fig. 5, a portion of the mesh is missing from the block structure. The missing blocks were removed on purpose as proper continuity could otherwise not be established. This problem is illustrated with a 2-dimensional schematic in Fig. 6. The blue, green and yellow rectangles represent the cortical, cancellous and marrow volumes respectively. The white block represents the problem region and blocks A and B both belong to the cortical volume. The pink node on block A represents the pink node in Fig. 5 and the dark blue node on block B represents the dark blue node in the same figure. The goal of this step is to generate a block structure that completes the cortical shell from A to B. It is not possible to use the white block to connect to block A as this would force direct connectivity between blocks A and B which would result in connectivity between the pink and dark blue nodes in Fig. 5, clearly creating severely ill shaped elements when studying Fig. 5. Instead, the white block was removed and replaced by two new blocks that were completely disconnected to the original block structure. While they had no connectivity to the original block structure they were connected to each other. Connectivity to the remaining block structure was created manually according to the arrows shown in Fig. 6(b). By replacing the white block with two blocks, the pink and dark blue nodes were separated by a distance allowing the blocks to better follow the geometry of the femur. This procedure of adding additional blocks was performed for the femoral head, the greater trochanter and at both of the condyles resulting in eight additional blocks.

Resulting mesh:

Once the additional eight blocks had been merged with the block-structure the mesh was complete and the density was easily increased. A mesh quality check found that a few elements had distorted angles. This was due to the free-formed geometry of the femur, where surfaces quickly change from convex to concave. One technique used to resolve this problem was to create internal pseudo points, curves and surfaces to which the internal blocks (elements) could be attached. This increased the control of those elements that were not otherwise directly constrained to the geometrical volumes. Another technique used to improve the mesh quality was to introduce bias by which the element spacing (within a block) could be controlled. Upon using these two techniques a high quality mesh was obtained. The element and nodes were divided into groups/sets. These sets were later used in defining material properties for the elements, and for applying boundary conditions and loads.

The mesh generated in True Grid consisted of 8832 eight-noded hexahedral elements with a total of 9505 nodes. This mesh was imported into Abaqus Standard (Abaqus Inc.), a commercially available FE software package, where the element type C3D8, a three-dimensional linear stress-element type, was chosen.

2.4. Material properties

Material properties of the femur used by other researchers vary slightly. The elastic isotropic cortical bone values used in this study are from [27], the cancellous bone values are based on the average value by [27], and the material properties for the bone marrow were obtained from [28]. The material definition can easily be modified to include the orthotropic behavior of the bone. The modulus of elasticity and Poisson's ratio used for the different segments are presented in Table 1.

2.5. Boundary conditions and loads

The femur was constrained at the distal end of the condyles to hinder motion in all degrees of freedom resembling the contact with the tibia. The loading condition consisted of the joint reaction force distributed at the femoral head and the abductor muscle force distributed on the greater

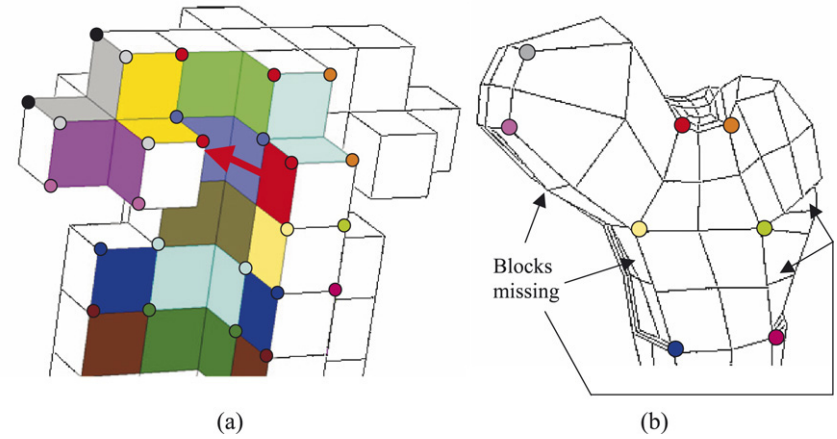

Fig. 5. Block-structure at femoral head before (a) and after (b) application of the block-boundary commands.

trochanter. This is the standard simplified loading scenario used by researchers [23,27,29]. Fig. 7 shows a sketch of the loading conditions. The magnitude and directions of the forces are reported in Table 2, where the x-, y-, and z-axes are along the medial/lateral, posterior/anterior, and superior/inferior directions, respectively.

3. Results

The femoral bone was subjected to a joint reaction force on the femoral head and an abductor muscle force at the greater trochanter. The stresses and displacements of the femoral model were obtained using a standard FE software package, Abaqus Standard (Abaqus Inc.). The highest von Mises stress (37 MPa) was recorded for a location on the medial side of the femur, directly distal to the femoral head in the cortical volume, as shown in Fig. 8. As the femoral head acts as a cantilever beam it causes high compressive stresses at this location, resulting in high von Mises stresses. In addition, compression due to gravity also contributes to the high stress value and the change in geometry creates stress concentrations that further add to the value. Both femoral neck fractures and intertrochanteric fractures initiate at the highest von Mises stresses location, further validating the present results.

Although it is known that von Mises stresses are not adapted for the behaviour of biological tissues, being a failure criterion for ductile metals, most results pertaining to FE studies of bones are given in terms of von Mises stresses. For easier comparison, the stresses here are also presented in terms of the von Mises effective stress.

The largest displacement magnitude of 3.1 mm is located at the superior end of the femur where no constraints are applied. The medial/lateral displacements, with a maximum value of 2.6 mm, are largest in close proximity to the load applications and are almost non-existent in the inferior half of the femur. The greater trochanter has the largest posterior displacement of 1.7 mm. The femoral head has a 1 mm displacement in the inferior direction while the greater trochanter has a superior displacement of 0.35 mm. This "rotating effect" is the cause of the opposing inferior/superior components of the applied joint and muscle loads. Overall, the displacements are largest close to the load applications and are reduced for locations further away; a zero displacement is obtained at the distal end of the condyles, verifying proper functionality of boundary conditions.

Table 1
Material properties

	Cortical bone	Cancellous bone	Bone marrow
E (MPa)	17,000	750	300
υ	0.33	0.33	0.45

Table 2
Applied loads

	x	y	z
Joint reaction force ($F1$) (N)	−616	171	−2800
Abductor muscle force ($F2$) (N)	430	0	1160

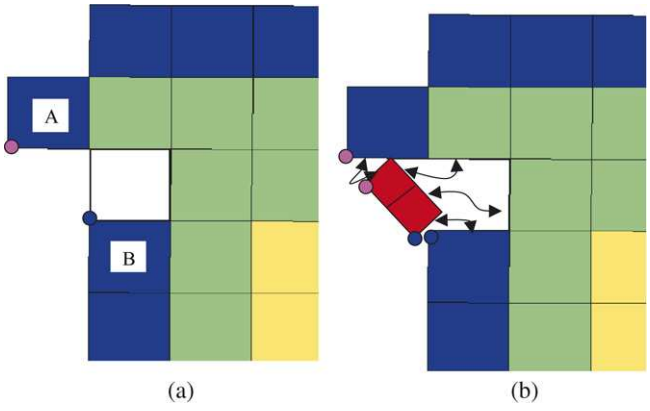

Fig. 6. Block structure in problem region.

4. Suggestions for hexahedral mesh development

A study has been presented providing a detailed outline of the steps taken in obtaining a high quality hexahedral FE model of the human femur. In developing this model, lessons were learned and this section provides suggestions that can minimize errors and help others better plan their modelling strategy.

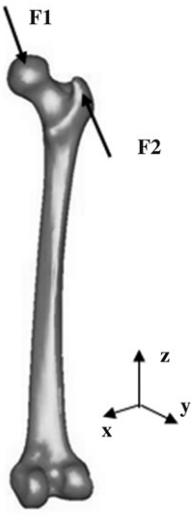

Fig. 7. Femoral loads.

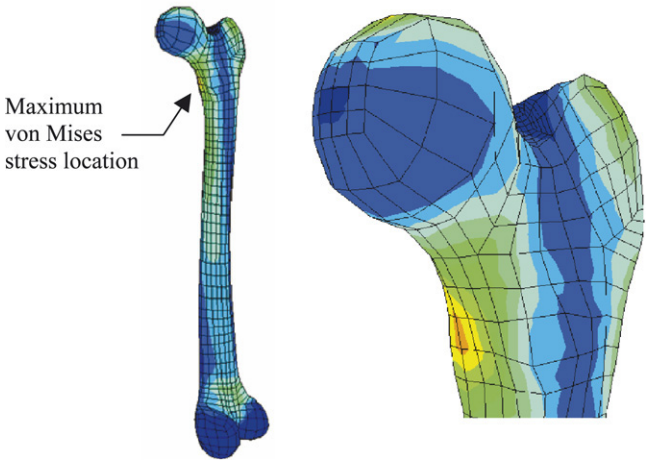

Fig. 8. Von Mises stress distribution.

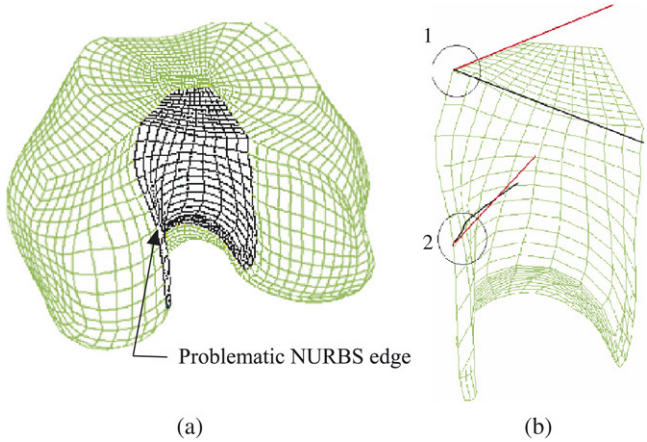

Fig. 9. Intersecting faces as a result of poorly chosen locations of the NURBS edges.

1. In obtaining the CT-data make sure the CT-data is in a format that the software can read. Different types of CT-data formats exist.
2. When smoothing geometry, make sure to remove very small surfaces. In some cases surfaces may be slivers of only a few micrometers. These surfaces can be removed by allowing an adjacent surface to grow into that region.
3. Before developing NURBS surfaces plan what the FE structure is going to look like. One should have a clear understanding of the block structure before finalizing the NURBS surface as the block structure will be attached/projected onto the patches that make up the NURBS surface. It is suggested that one completely control the location of the NURBS lines/patch edges, as shown in Fig. 3, rather than using the default NURBS. When placing the NURBS lines, pay attention to concavity and convexity. The outermost blocks will be projected onto this NURBS surface and if the edge of a block changes drastically from convex to concave, the inner surfaces of the blocks may cut through the outer surface of the block. Fig. 9 illustrates the problem that can result from not positioning the NURBS lines in a well planned location. The black lines in Fig. 9(b) belong to a face of the black block in Fig. 9(a) which is projected onto the geometry while the red lines of the block belong to another face of the block which is not controlled by geometry. As the curvature of the outer face changes drastically with the geometry, while the inner (non-controlled) face stays straight, the two surfaces intersect (location 2), resulting in poorly defined elements. To minimize the risk of this type of problem, it is suggested that the NURBS edge be located where this rapid change in curvature does not exist. For the case at hand the problem was resolved by moving the NURBS edge to the right. It may also be recommended to use more patches and blocks to minimize this problem. If this problem cannot be avoided, it is suggested that pseudo surfaces be developed to steer the inner-block faces away from the geometry-controlled faces.
4. One of the challenges in creating hexahedral meshes using a multi-block mesher is to determine how to properly decompose the structure into blocks, here referred to as the block structure. However, the most time consuming task involves attaching the corners, edges and faces of the block structure to the geometry. For this reason, it is important that the complete block structure be determined before any attachments/projections are performed and preferably before the patches and NURBS are created. It is suggested that the block structure be thought of as a block of clay for which portions (blocks) are carved away where not needed. For ease of checking validity of the model it is also suggested that one builds a portion of the mesh at a time and then go back to make modifications to the block structure by adding volumes to the mesh. In determining the number of blocks to use, one should look at the NURBS surface and count the individual patches. If, for example, the NURBS surface consists of 20 patches in one direction, 20 or 10 blocks can be recommended in that direction. If using fewer blocks than there are patches, the surfaces need to be combined into fewer surfaces.
5. Check the quality of the mesh as it is being developed, not only after completing it. If poorly defined elements are

detected, either make modifications to the NURBS structure in the affected region or control inner faces/edges/corners of the block structure as described in suggestion number three above. In some cases introducing bias in the element spacing may resolve the problem of poorly defined elements.

5. Discussion and conclusion

The objective of the current research was to develop a high fidelity model of the femoral bone using hexahedral elements such that future, more specific, analyses can be performed without having to redevelop a model from CT data. The model developed can easily be analysed under different loading conditions, modified to include more advanced material models and, if desired, a specific implant design.

As the model is based on data available to other researchers through the Visible Human Project at the National Institutes of Health, the results obtained herein can be compared to those of other studies and can be verified by others. In addition to providing a model that can be used in numerous different types of studies, this work also provides a detailed description on how to develop a robust hexahedral FE model of human bones. The challenges of developing hexahedral FE models with free formed geometry are addressed within this paper as are methods on how to overcome those challenges. For some applications, such as contact analysis, hexahedral models perform much better than tetrahedral models and the procedure and results described herein should therefore be of great value to researchers attempting to develop other hexahedral meshes.

References

[1] Breckelmans WA, Poort HW, Slooff TJ. A new method to analyse the mechanical behaviour of skeletal parts. Acta Orthopaedica Scandinavica 1972;43(5):301–17.

[2] Little RB, Wevers HW, Siu D, Cooke TDV. A three dimensional finite element analysis of the upper tibia. Journal of Biomechanical Engineering 1986;(108):111–9.

[3] Rajani S, Mehta BV. Three dimensional modeling and finite element analysis of the tibia. IEEE; 1994.

[4] Wirtz DieterChristian, Pandorf Thomas, Portheine Frank, Radermacher Klaus, Schiffers Norbert, Prescher Andreas, et al. Concept and development of an orthotropic FE model of the proximal femur. Journal of Biomechanics 2003;36:289–93.

[5] Spears IR, Pfeiderer Martin, Schneider Erich, Hille Ekkehard, Morlock MM. The effect of interfacial parameters on cup-bone relative micromotions: A finite element investigation. Journal of Biomechanics 2001;34:113–20.

[6] Greer B, Wang E, Jiang Y. On the appropriateness of using the standardized femur for FEA in the proximal region. In: 1999 Summer bioengineering conference, vol. 42. ASME, BED; 1999. p. 669–670.

[7] Beek M, Koolstra JH, van Ruijven LJ, van Eijden TMGJ. Three-dimensional finite element analysis of the human temporomandibular joint disc. Journal of Biomechanics 2000;33(3):307–16.

[8] Nadzadi ME, Pedersen DR, Yack HJ, Callaghan JJ, Brown TD. Kinematics, kinetics, and finite element analysis of commonplace maneuvers at risk for total hip dislocation. Journal of Biomechanics 2003;36(4):577–91.

[9] Cheung J, Zhang M, Leung A, Fan Y. Three-dimensional finite element analysis of the foot during standing—a material sensitivity study. Journal of Biomechanics 2004;38(5):1045–54.

[10] Jia Xiaohong, Zhang Ming, Lee WCC. Load transfer mechanics between trans-tibial prosthetic socket and residual limb-dynamic effects. Journal of Biomechanics 2004;37(9):1371–7.

[11] Perillo-Marcone A, Ryd L, Johnsson K, Taylor M. A combined RSA and FE study of the implanted proximal tibia: Correlation of the post-operative mechanical environment with implant migration. Journal of Biomechanics 2004;37(8):1205–13.

[12] Iesaka K, Tsumura H, Sonoda H, Sawatari T, Takasita M, Torisu T. The effects of tibial component inclination on bone stress after unicompartmental knee arthroplasty. Journal of Biomechanics 2002;35(7):969–74.

[13] Teller Seth. Mesh generation computer graphics group, Massachusetts Institute of Technology; Available: http://graphics.lcs.mit.edu/~seth/pubs/taskforce/section3_7.html.

[14] Abaqus Inc. Analysis Manual, Volume IV: Elements, section 14.1.1-5. Version 6.4. www.abaqus.com.

[15] Cifuentes AO, Kalbag A. A performance study of tetrahedral and hexahedral elements in 3-D finite element structural analysis. Finite Elements in Analysis and Design 1992;12:313–8.

[16] Benzley SE, Ernest Perry, Karl Merkley, Brett Clark, Greg Sjaardema. A comparison of all-hexahedral and all-tetrahedral finite element meshes for elastic and elasto–plastic analysis. In: Proceedings, 4th international meshing roundtable, Sandia National Laboratories; 1995. p. 179–91.

[17] Element Selection Appendix 2. Introduction to Abaqus training course documentation. Course information available: http://www.abaqus.com/support/sup_seminar_desc.html.

[18] Ionescu Irina, Conway Ted, Schonning Alexandra, Almutairi Mutlaq, Nicholson DW. Solid modeling and static finite element analysis of the human tibia, 2003 Summer bioengineering conference 2003.

[19] Cody DD, Gross GJ, Hou FJ, Spencer HJ, Goldstein SA, Fyhrie DP. Femoral strength is better predicted by finite element models than QCT and DXA. Journal of Biomechancis 1999;32:1013–20.

[20] Waide V, Cristofolini L, Stolk J, Verdonschot N, Boogaard GJ, Toni A. Modeling the fibrous tissue layer in cemented hip replacements: Experimental and finite element methods. Journal of Biomechanics 2004;37:13–26.

[21] Viceconti Marco, Davinelli Mario, Taddei Fulvia, Cappello Angelo. Automatic generation of accurate subject-specific bone finite element models to be used in clinical studies. Journal of Biomechanics 2004;37:1597–605.

[22] Duda G, Heller M, Albinger J, Schulz O, Schneider E, Claes L. Influence of muscle forces on femoral strain distribution. Journal of Biomechanics 1998;31:841–6.

[23] Wang CJ, Yettram AL, Yao MS, Procter P. Finite element analysis of a Gamma nail within a fractured femur. Medical Engineering and Physics 1998;20:677–83.

[24] Visible human male. Available: http://www.nlm.nih.gov/research/visible/visible_human.html.

[25] Jackson Simon, Thomas Richard. Cross sectional imaging made easy, Churchill Livingstone, Available: http://www.harcourt-international.com/e-books/pdf/940.pdf; 2004.

[26] Rüegsegger Peter. Imaging of bone structure. In: Cowin, SC editor. Bone mechanics handbook, 2nd ed., Boca Raton, London, New York, Washington, D.C.

[27] Taylor ME, Tanner KE, Freeman MAR, Yettram AL. Stress and strain distribution within the intact femur: Compression or bending? Medical Engineering and Physics 1996;18(2):122–31.

[28] Kasra M, Grynpas M. Finite element dynamic response analysis of trabecular bone: Effect of bone marrow. Advances in bioengineering, vol. 28. BED ASME; 1994. p. 225–7.

[29] Sitthiseripratip K, Van Oosterwyck H, Vander Sloten J, Mahaisavariya B, Bohez ELJ, Suwanprateeb J, et al. Finite element study of trochanteric gamma nail for trochanteric fracture. Medical Engineering and Physics 2003;25(2):99–106.